JOURNAL OF MATERIALS SCIENCE **40** (2005) 129–133

Electrical properties of $MREGeO_4$ (M = Li, Na, K; RE = rare earth) ceramics

YAN LIN AUNG, S. NAKAYAMA
Department of Applied Chemistry and Biotechnology, Niihama National College of Technology, Niihama 792-8580, Japan
E-mail: nakayama@chem.niihama-nct.ac.jp

M. SAKAMOTO
Department of Material & Biological Chemistry, Faculty of Science, Yamagata University, Yamagata 990-8560, Japan

Fourteen kinds of alkali-metal rare earth germanate ceramics, $MREGeO_4$ (M = Li, Na, K; RE = rare earth), were synthesized and their electrical properties were investigated. The crystal structures of the major phases of $MREGeO_4$ could be classified into four groups; hexagonal (apatite type), tetragonal, orthorhombic (olivine type) and orthorhombic (β-K_2SO_4 type). The tetragonal group exhibited higher ionic conductivity than the other groups in the range 300 to 700°C. The highest conductivity was achieved for the $LiNdGeO_4$ having a tetragonal structure (2.95×10^{-2} S cm^{-1} at 700°C). Analyses on the basis of the Nernst's equation indicated that the two electron reaction associated with carbon dioxide molecule takes place at the detection electrode above 400°C regardless of the kind of electrolyte. The electromotive force, EMF, of the potentiometric CO_2 gas sensors designed using $MLaGeO_4$ (M = Li, Na, K) increased linearly with an increase in the logarithmic value of CO_2 partial pressure, in accordance with the Nernst equation.

1. Introduction

With the development of solid-state batteries and chemical sensors, ionic conductors (solid-state electrolytes) which have higher electrical conductivity and a higher degree of densification are becoming increasingly important because of their suitability for the main components of such batteries and sensors [1, 2]. To develop and improve such ionic conductors, the choice of crystal structures and mobile ions, the addition of modifier ion species and the methods used to increase their density have to be considered [3, 4]. Among the many alkali-metal ionic conductors, β-eucryptite, $LiAlSiO_4$ is known as a Li ionic conductor possessing a conducting pathway along the minor axis of the hexagonal structure, in which a three-dimensional network is built from interconnected AlO_4 and SiO_4 tetrahedra [5]. Another characteristic of $LiAlSiO_4$ is a fairly higher resistance to water; when 10 *g* of a sample sintered at 1300°C was immersed in 100 ml of water at room temperature for 24 h, only 22 ppm of Li^+ ion was eluted [6]. In order to develop well compacted alkali-metal ionic conductors with excellent water-resistance and high ionic conductivity, we previously prepared alkali-metal (M) rare-earth (RE) silicates ($MRESiO_4$) and investigated their ionic electrical conductivities [7, 8]. These materials can be thought of as a three-dimensional network of interconnected REO_6 octahedra and SiO_4 tetrahedra i.e., using a series of rare earth elements instead of aluminium in $LiAlSiO_4$. It was found that the major phase of $MRESiO_4$ (M = Li, K; RE = La, Nd, Sm, Gd, Dy) ceramics had the hexagonal apatite type structure (space group:P63/m) [9] and these alkali-metal ionic conductors exhibited higher electrical conductivities [10, 11].

In this work, we synthesized alkali based $MREGeO_4$ (M = Li, Na, K; RE = La, Pr, Nd, Sm, Gd, Dy, Ho, Er, Yb) ceramics in which Ge (ionic radius: 0.040 nm [12]) was substituted for Si (ionic radius: 0.026 nm [12]) in the SiO_4 tetrahedra, in order to gain an information about the size effect of the tetrahedral site. The crystal structures and the electrical properties of these ceramics, compared with $MRESiO_4$ (M = Li, Na, K) ceramics previously reported [8] were investigated.

2. Experimental

Reagent grade M_2CO_3 (M = Li, Na, K), GeO_2 and rare-earth oxide RE_2O_3 (RE = La, Nd, Sm, Gd, Dy, Ho, Er, Yb) or Pr_6O_{11} were ball-milled in a plastic pot with zirconia balls and methanol for 16 h. The mixture was dried in an oven at 80°C and was put into an alumina crucible and calcined in air at 800°C for 2 h. The resultant powder was ball-milled again for 16 h into a fine powder. After being dried, the powder was pressed at 50 MPa into a disc and sintered on a platinum plate at 1050–1150°C (see Table I).

The densities of the sintered products were determined by Archimedes method. The powder X-ray

TABLE I Lattice constants, cell volumes, phases and sintering temperatures

Material	a (nm)	b (nm)	c (nm)	V (nm^3)	Phase[a]	Sintering temp. (°C)
			$MREGeO_4$ system			
$LiLaGeO_4$	0.987		0.723	0.609	H(a)	1050
$LiPrGeO_4$	0.975		0.709	0.583	H(a)	1050
$LiNdGeO_4$	0.742		0.974	0.536	T	1100
$LiSmGeO_4$	0.735		0.965	0.521	T	1100
$LiGdGeO_4$	0.730		0.961	0.512	T	1100
$LiDyGeO_4$	0.507	1.110	0.633	0.354	O(o)	1100
$LiHoGeO_4$	0.507	1.110	0.631	0.353	O(o)	1150
$LiErGeO_4$	0.504	1.110	0.633	0.352	O(o)	1150
$LiYbGeO_4$	0.502	1.094	0.625	0.343	O(o)	1150
$NaLaGeO_4$	0.556	1.015	0.711	0.401	O(k)	1100
$NaNdGeO_4$	0.550	1.011	0.693	0.385	O(k)	1300
$NaSmGeO_4$	0.544	1.036	0.675	0.380	O(k)	1100
$KLaGeO_4$	0.989		0.732	0.620	H(a)	1150
$KSmGeO_4$	0.581	0.857	0.813	0.405	O(k)	1300
			$MRESiO_4$ system			
$LiLaSiO_4$	0.969		0.715	0.582	H(a)	1000
$LiNdSiO_4$	0.951		0.699	0.552	H(a)	1000
$LiSmSiO_4$	0.945		0.691	0.537	H(a)	1000
$LiDySiO_4$	0.936		0.676	0.514	H(a)	1000
$LiHoSiO_4$	0.499	1.081	0.633	0.336	O(o)	1050
$LiErSiO_4$	0.500	1.083	0.630	0.335	O(o)	1200
$LiYbSiO_4$	0.493	1.072	0.624	0.327	O(o)	1300
$NaLaSiO_4$	0.541	0.948	0.715	0.369	O(k)	1250
$NaNdSiO_4$	0.539	0.944	0.699	0.353	O(k)	1250
$NaSmSiO_4$	0.535	0.940	0.688	0.346	O(k)	1250
$KLaSiO_4$	0.971		0.724	0.591	H(a)	1350
$KSmSiO_4$	0.946		0.701	0.543	H(a)	1350

[a]H(a) = hexagonal (apatite type), T = tetragonal, O(o) = orthorhombic (olivine type) and O(k) = orthorhombic (β-K_2SO_4 type).

diffraction (XRD) measurements were carried out using Cu K_α radiation in the 2θ range of 20 to 60°. After being coated on both sides of the disc with Pt paste, they were baked at 1000°C. The electrical properties were measured in the temperature range of 300 to 700°C, using an impedance-analyzer (HP4194A) in the frequency range of 100 to 10 MHz.

The solid state cell as a CO_2 gas sensor is composed of the following ionic conductor and electrodes:

$$(-)\ \text{air, Pt}|\text{MLaGeO}_4\ (\text{M} = \text{Li, Na, K})|\text{Au, } M_2CO_3,\ CO_2, O_2\ (+)$$

$MLaGeO_4$ (M = Li, Na, K) discs were prepared as above then one side was coated with a Pt paste and the other with a Au paste, before the disc was baked at 1000°C. Then, both sides of the disc were connected with Pt wires. An aqueous solution of M_2CO_3 was applied to the Au detection electrode and the electrode was dried to prepare the solid electrode. The sensor thus designed was fixed on one-end of an alumina pipe with a glass cement so that the Pt counter electrode was on the inside.

The response characteristics were measured using four kinds of standard CO_2 gases with partial pressures of 1×10^0, 1×10^1, 1×10^2 and 1×10^3 Pa, prepared by diluting given amounts of CO_2 with a synthetic air ($<2 \times 10^{-1}$ Pa CO_2) purchased from Sumitomo-Seika Inc. Electromotive force, EMF, was measured using an Advantest TR8652 electrometer.

3. Results and discussion

3.1. Crystal structure

Each sample assumed the characteristic color of the component rare earth ion; colorless for the La, Gd, Dy and Yb ceramics, pale yellow for the Sm ceramics, green for the Pr ceramics, greenish yellow for the Ho ceramics and pink for the Er ceramics.

Typical XRD patterns of $MREGeO_4$ (M = Li, Na, K; RE = La, Pr, Nd, Sm, Gd, Dy, Ho, Er, Yb) are shown in Fig. 1. The crystal structures of the major phase of $MREGeO_4$ were classified into four

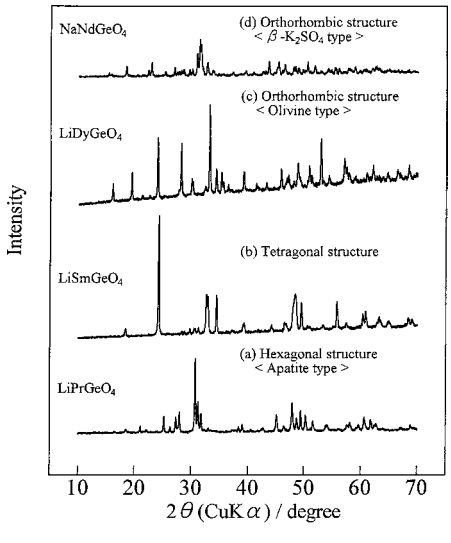

Figure 1 Typical XRD patterns of: (a) hexagonal apatite-type $LiPrGeO_4$, (b) tetragonal $LiSmGeO_4$, (c) orthorhombic olivine-type $LiDyGeO_4$, and (d) orthorhombic β-K_2SO_4-type $NaNdGeO_4$.

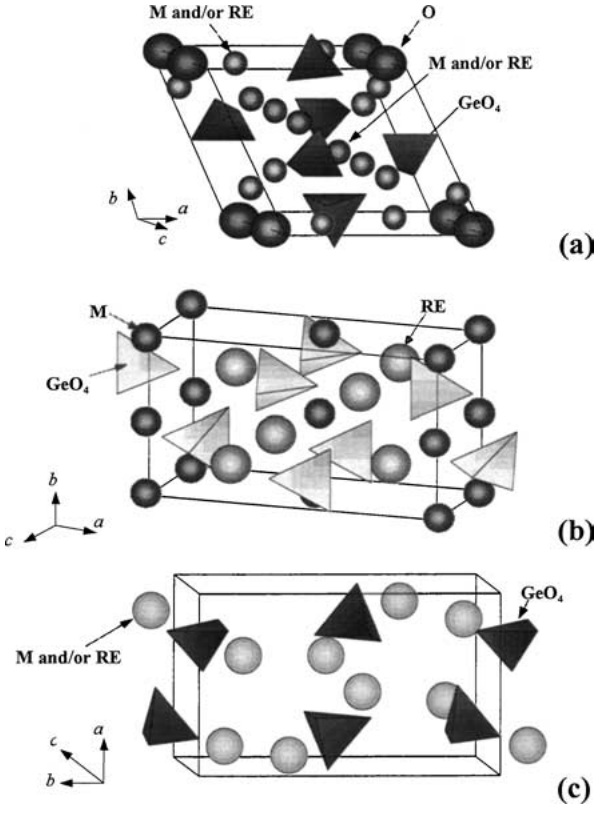

Figure 2 (a) Apatite-type crystal structure of $MRE_9(GeO_4)_6O_2$ proposed for the major phase of $LiREGeO_4$ (RE = La ~ Pr) and $KLaGeO_4$, (b) olivine-type crystal structure of $LiREGeO_4$ (RE = Dy ~ Yb), and (c) β-K_2SO_4-type crystal structure of $NaREGeO_4$ (RE = La, Nd, Sm) and $KSmGeO_4$.

groups: hexagonal (apatite type) for $LiREGeO_4$ (RE = La-Pr) and $KLaGeO_4$ [13], tetragonal for $LiREGeO_4$ (RE = Nd-Gd) [13], orthorhombic (olivine type) for $LiREGeO_4$ (RE = Dy-Yb) [13], orthorhombic (β-K_2SO_4 type) for all of $NaREGeO_4$ (RE = La-Sm), hexagonal (apatite type) for $KLaGeO_4$ and orthorhombic (β-K_2SO_4 type) for KSmGeO4 (see Table I). Fig. 2 shows the structural illustrations of hexagonal apatite type, orthorhombic olivine-type and orthorhombic β-K_2SO_4 type crystals.

The lattice parameters calculated from the XRD patterns of the $MREGeO_4$ system are also summarized in Table I, together with those of the $MRESiO_4$ system. The substitution of Ge^{4+} with an ionic radius of 0.040 nm for Si^{4+} with an ionic radius of 0.026 nm is reflected in the increase of cell volume, when $MREGeO_4$ and $MRESiO_4$ of the same structure are compared. Hexagonal apatite type $MLaGeO_4$(M = Li, K) and orthorhombic olivine type $LiREGeO_4$ (RE = Ho, Er, Yb) have cell volumes of 0.609–0.620 nm^3 and 0.353–0.343 nm^3, respectively, which are increased by ca. 5% compared with those of the corresponding $MLaSiO_4$ (M = Li, K) and $LiRESiO_4$ (RE = Ho, Er, Yb). The cell volumes of orthorhombic β-K_2SO_4 type $NaREGeO_4$ (RE = La, Nd, Sm) are in the range of 0.401–0.380 nm^3, which are 9–10% larger than those of the corresponding $NaRESiO_4$.

3.2. Electrical properties

In order to determine the conductivity, complex plane impedance analysis was performed. The typical complex impedance plot at the lower temperature gave a semicircle which passes through the x-axis near the origin. As the temperature was raised, the semicircle, probably corresponding to the electrolyte itself, diminished and a spike, probably arising from the electrolyte-electrode behavior, was observed in the lower frequency region. From these results, the conductivity was determined by the extrapolation to zero reactance of the complex impedance plot. The conductivity data were analysed using the Arrhenius Equation 1.

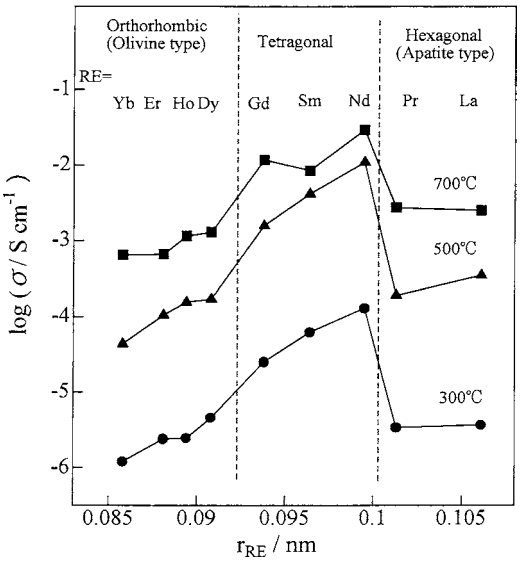

Figure 3 Relationship between the ionic radii of RE^{3+} and the electrical conductivities of $LiREGeO_4$.

$$\sigma T = \sigma_0 \exp(-E/kT) \quad (1)$$

where σ, σ_0, E, k and T are the conductivity, pre-exponential factor, activation energy, Boltzmann constant and absolute temperature, respectively.

Fig. 3 shows plots of the logarithmic conductivity values of $LiREGeO_4$ at 300, 500 and 700°C against the ionic radii of the rare earths. The conductivity increased with the rise of temperature, when the same rare earth was used. At a given temperature, the conductivity increased with the increase in ionic radius of RE^{3+} from Yb to Nd and a steep drop was observed for Pr and La. Conductivities of $LiLaGeO_4$ and $LiPrGeO_4$ are lower than $LiNdGeO_4$ by 1.5 orders of magnitude at 300 and 500°C and one order of magnitude at 700°C. The tetragonal family exhibited higher conductivities than the orthorhombic and hexagonal families in the temperature range of 300 to 700°C. The highest conductivity of 2.95×10^{-2} S cm^{-1} was achieved for the tetragonal $LiNdGeO_4$ at 700°C.

Arrhenius plots of $NaREGeO_4$ (RE = La, Nd, Sm) and $KREGeO_4$ (RE = La, Sm) are shown in Fig. 4. The conductivities of orthorhombic β-K_2SO_4 type $NaREGeO_4$ (RE = La, Nd, Sm) were higher than those of hexagonal apatite type $KLaGeO_4$ and orthorhombic β-K_2SO_4 type $KSmGeO_4$.

The effect of alkali metal on the conductivity was examined at 400, 500 and 600°C using $MLaGeO_4$ (M = Li, Na, K). Results are summarized in Fig. 5 which also shows the data of $MLaSiO_4$ previously

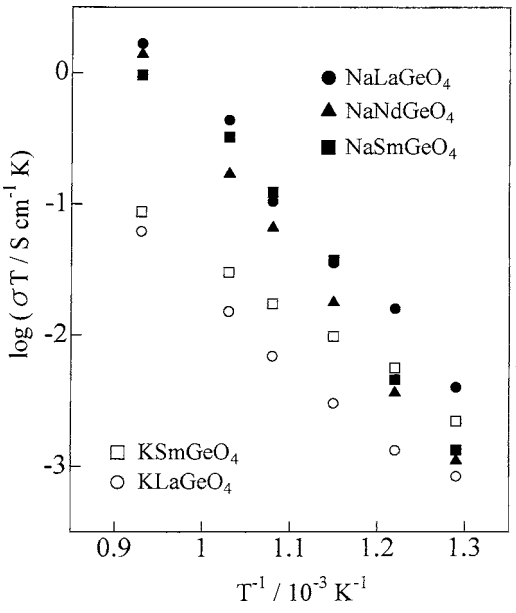

Figure 4 Arrhenius plots for $NaREGeO_4$ and $KREGeO_4$.

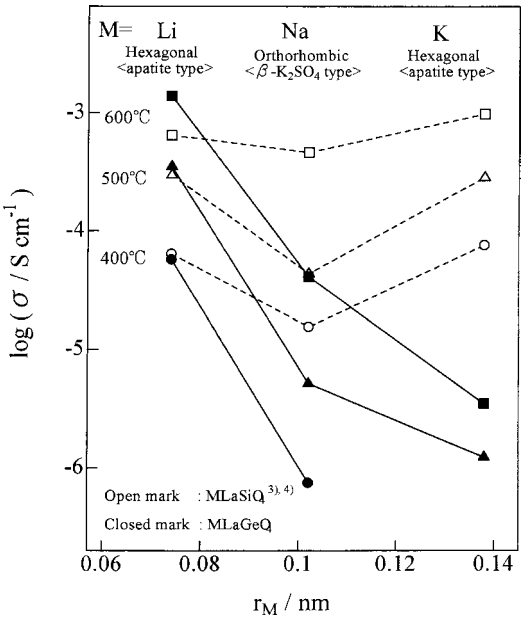

Figure 5 Relationship between the ionic radii of alkali-metal and the conductivities of $MLaGeO_4$ and $MLaSiO_4$ (M = Li, Na, K).

reported [8]. The conductivity of $MLaGeO_4$ increased with the decrease in ionic radius of alkali metal at all temperatures, whereas the previous $MLaSiO_4$ gave the minimum value for M = Na [8]. Furthermore, the conductivities of $NaLaGeO_4$ and $KLaGeO_4$ are lower by 1–2.5 orders of magnitude than those of $NaLaSiO_4$ and $KLaSiO_4$ [8]. These lower conductivities cannot be explained by the estimation that the cell volumes of $NaLaGeO_4$ and $KLaGeO_4$ are 8.7 and 4.9% larger than those of $NaLaSiO_4$ and $KLaSiO_4$, respectively, since the larger cell volume is generally thought to increase the mobility of the alkali metal ion.

3.3. Response characteristics as a CO_2 gas sensor

Fig. 6 shows the dependence of EMF on the logarithm of CO_2 partial pressure, $\log P_{CO_2}$, at 500°C for the CO_2

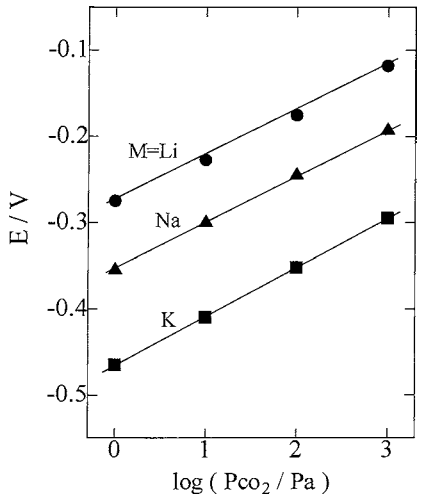

Figure 6 Plots of the sensor EMF as a function of the logarithms of CO_2 partial pressures at 500°C.

gas sensors designed using $MLaGeO_4$ (M = Li, Na or K). Standard gases were passed through the detection electrode side of the sensors at a flow rate of 50 cm^3 min^{-1}. The EMF of each sensor decreased with increase in $\log P_{CO_2}$ and the dependence of EMF on $\log P_{CO_2}$ obeyed the Nernst equation. In the present apparatus, potentials at a given temperature are almost constant, as the counter electrode is shielded from the detected gas. This indicates that the EMF change is due to the potential change at the detection electrode and hence the electron transfer number at the detection electrode can be estimated from the slope of the straight lines given in Fig. 6. Table II summarizes the estimated slopes and electron transfer numbers, n, which can be approximated as 2 above 400°C, suggesting that the detection above 400°C is accomplished based on the two electron transfer reaction associated with one CO_2 molecule.

The response mechanism of the present CO_2 gas sensor was investigated. The counter electrode is always exposed to a constant atmosphere of 2.1×10^4 Pa oxygen partial pressure, and therefore the electrode reaction can be expressed by the following equation.

$$2M^+ + 1/2O_2 + 2e^- = M_2O \qquad (2)$$

On the other hand, it is assumed that the following reaction occurs at the detection electrode.

$$2M^+ + CO_2 + 1/2O_2 + 2e^- = M_2CO_3 \qquad (3)$$

When the Nernst equation is applied to the above Equations 2 and 3, the potentials of counter electrode,

TABLE II Slopes of sensor EMF vs. log P_{CO_2} and electron transfer numbers (n)

	slope/mV decade^{-1}			
Electrolyte	300°C	400°C	500°C	600°C
$LiLaGeO_4$	45.0 (2.5)	57.5 (2.3)	70.0 (2.2)	90.0 (1.9)
$NaLaGeO_4$	41.5 (2.8)	60.0 (2.2)	70.0 (2.2)	85.4 (2.2)
$KLaGeO_4$	15.0 (7.6)	65.0 (2.1)	72.5 (2.1)	71.0 (2.4)

Ec, and detection electrode, Es, are expressed by the following equations, respectively:

$$Ec = Ec' - (RT/2F)\ln\left(a_{M_2O}/a_{M^+}^2 \cdot \left(P_{O_2}^{I}\right)^{1/2}\right) \quad (4)$$

$$Es = Es' - (RT/2F)\ln\left(a_{M_2CO_3}/a_{M^+}^2 \cdot \left(P_{O_2}^{II}\right)^{1/2} \cdot P_{CO_2}\right) \quad (5)$$

where E', R, T, F, $a_{M_2CO_3}$, a_{M_2O}, P_{CO_2} and P_{O_2} are standard electrode potential, gas constant, absolute temperature, Faraday constant, activities of M_2CO_3 and M_2O, and partial pressures of CO_2 and O_2, respectively. As both Ec' and Es' are constant, the EMF, abbreviated as E, is expressed as follows:

$$\begin{aligned} E &= Es - Ec \\ &= E' - (RT/2F)\ln\left(a_{M_2CO_3} \cdot \left(P_{O_2}^{I}\right)^{1/2}/a_{M_2O}\right. \\ &\quad \left. \cdot P_{CO_2} \cdot \left(P_{O_2}^{II}\right)^{1/2}\right) \end{aligned} \quad (6)$$

where E' is a constant. When the activities of M_2CO_3, M_2O, $P_{O_2}^{I}$ and $P_{O_2}^{II}$ are kept constant, the CO_2 concentration can be calculated from E. Undoubtedly, the present results can be explained by this Equation 6, as can be seen in Fig. 6.

4. Conclusion

A series of $MREGeO_4$ (M = Li, Na, K; RE = rare earth) ceramics were synthesized, and their crystal structures and electrical properties were investigated. The results are summarized as follows;

(1) The crystal structures of the major phase of $LiREGeO_4$ ceramics could be classified into three groups: hexagonal (apatite type) for La-Pr, tetragonal for Nd-Gd and orthorhombic (olivine type) for Dy-Yb. The crystal structure of $NaREGeO_4$ ceramics (RE = La-Sm) was orthorhombic (β-K_2SO_4type). The $KLaGeO_4$ and $KSmGeO_4$ ceramics have hexagonal (apatite type) and orthorhombic (β-K_2SO_4 type) structures, respectively.

(2) The substitution of Ge^{4+} with an ionic radius of 0.040 nm for Si^{4+} with an ionic radius of 0.026 nm was reflected in the increase in cell volume. The cell volume of the $MREGeO_4$ was about 5% greater than the $MRESiO_4$ with the same crystal structure.

(3) In the $LiREGeO_4$ ceramics, the tetragonal family exhibited higher ionic conductivities than the other families in the temperature range of 300 to 700°C and the $LiNdGeO_4$ having a tetragonal structure, showed the highest conductivity (2.95×10^{-2} S cm^{-1}) at 700°C. The conductivity of $MLaGeO_4$ increased with decreasing ionic radius of alkali-metal.

(4) The EMF values of the potentiometric CO_2 gas sensors prepared using $MLaGeO_4$ (M = Li, Na or K) were correlated with the CO_2 concentrations by the Nernst equation. The number of electrons transferred was estimated to be 2 above 400°C. The response characteristics of the sensor were not influenced by the type of solid electrolyte.

References

1. S. ITO, K. UI, N. KOURA and K. AKASHI, *Solid State Ion.* **113–115** (1998) 17.
2. S. NAKAYAMA and Y. SADAOKA, *J. Mater. Chem.* **4** (1994) 663.
3. M. G. ALEXANDER, *Solid State Ion.* **22** (1987) 257.
4. H. AONO and N. IMANAKA, *Acc. Chem. Res.* **27** (1994) 265.
5. U. V. ALPEN, E. SCHONHERR, H. SCHULZ and G. H. TALAT, *Electrochimica Acta* **22** (1977) 805.
6. S. NAKAYAMA, H. KUROSHIMA, Y. SADAOKA and Y. SAKAI, *J. Ceram. Soc. Jpn.* **100** (1992) 968.
7. S. NAKAYAMA and M. SAKAMOTO, *ibid.* **100** (1992) 867.
8. S. NAKAYAMA and Y. SADAOKA, *J. Mater. Chem.* **3** (1993) 1251.
9. J. FELSCHE, *J. Solid State Chem.* **5** (1972) 266.
10. M. SATO, Y. KONO, H. UEDA, K. UEMATSU and K. TODA, *Solid State Ion.* **83** (1996) 249.
11. H. MATSUMOTO, K. YONEZAWA and H. IWAHARA, *ibid.* **113–115** (1998) 79.
12. R. D. SHANNON and O. T. PREWITT, *Acta Cryst.* B **25** (1969) 925.
13. JCPDS No. 32-567, JCPDS No. 20-643, JCPDS No.20-1116.

Received 16 October 2003
and accepted 19 July 2004